Mon. Not. R. Astron. Soc. **000**, 1–14 (2012) Printed 25 June 2013 (MN LATEX style file v2.2)

Star/galaxy separation at faint magnitudes: Application to a simulated Dark Energy Survey

M. T. Soumagnac [1⋆], F. B. Abdalla[1⋆], O. Lahav[1⋆], D. Kirk[1], I. Sevilla[2], E. Bertin[3], B. T. P. Rowe[1], J. Annis[4], M. T. Busha[5,6], L. N. Da Costa[7,8], J. A. Frieman[4,9,10], E. Gaztanaga[11], M. Jarvis[12], H. Lin[4], W. J. Percival[13], B. X. Santiago[8,14], C. G. Sabiu[15], R. H. Wechsler[16,17], L. Wolz[1,18], B. Yanny[4].

[1] *Department of Physics and Astronomy, University College London, Gower Street, London WC1E6BT, UK*
[2] *Centro de Investigaciones Energeticas Medioambientales y Tecnologicas, Av.Complutense 40, 28040 Madrid, Spain*
[3] *Institut d'Astrophysique de Paris, UMR 7095 CNRS, Universite Pierre et Marie Curie, 98 bis boulevard Arago, F-75014 Paris, France*
[4] *Center for Particle Astrophysics, Fermi National Accelerator Laboratory, P.O. Box 500, Batavia, IL 60510, USA*
[5] *Institute for Theoretical Physics, University of Zurich, Zurich, Switzerland*
[6] *Physics Division, Lawrence Berkeley National Laboratory, Berkeley, CA, USA*
[7] *Observatorio Nacional, Rua Gal. Jose Cristino 77, Rio de Janeiro, RJ - 20921-400, Brazil*
[8] *Laboratorio Interinstitucional de e-Astronomia - LineA, Rua Gal. Jos e Cristino 77, Rio de Janeiro, RJ - 20921-400, Brazil*
[9] *Department of Astronomy and Astrophysics, The University of Chicago, 5640 South Ellis Avenue, Chicago, IL 60637, USA*
[10] *Kavli Institute for Cosmological Physics, The University of Chicago, 5640 South Ellis Avenue Chicago, IL 60637, USA*
[11] *Institut de Ciencies de lEspai (IEEC-CSIC), E-08193 Bellaterra (Barcelona), Spain*
[12] *Department of Physics and Astronomy, University of Pennsylvania, Philadelphia, PA 19104, USA*
[13] *Institute of Cosmology and Gravitation, University of Portsmouth, Portsmouth, PO1 3FX, UK*
[14] *Departamento de Astronomia, Universidade Federal do Rio Grande do Sul Av. Bento Goncalves 9500, Porto Alegre, RS 91501-970, Brazil*
[15] *Korea Institute for Advanced Study, Dongdaemun-gu, Seoul 130-722, Republic of Korea*
[16] *Kavli Institute for Particle Astrophysics and Cosmology, SLAC National Accelerator Laboratory, 2575 Sand Hill Rd., Menlo Park, CA 94025, USA*
[17] *Physics Department, Stanford University, Stanford, CA 94305, USA*
[18] *Sub-Department of Astrophysics, Department of Physics, University of Oxford, Keble Road, Oxford OX1 3RH, UK*

Accepted day– Month Date. Received year month date; in original form year month date

ABSTRACT

We address the problem of separating stars from galaxies in future large photometric surveys. We focus our analysis on simulations of the Dark Energy Survey (DES). In the first part of the paper, we derive the science requirements on star/galaxy separation, for measurement of the cosmological parameters with the Gravitational Weak Lensing and Large Scale Structure probes. These requirements are dictated by the need to control both the statistical and systematic errors on the cosmological parameters, and by Point Spread Function calibration. We formulate the requirements in terms of the *completeness* and *purity* provided by a given star/galaxy classifier. In order to achieve these requirements at faint magnitudes, we propose a new method for star/galaxy separation in the second part of the paper. We first use Principal Component Analysis to outline the correlations between the objects parameters and extract from it the most relevant information. We then use the reduced set of parameters as input to an Artificial Neural Network. This multi-parameter approach improves upon purely morphometric classifiers (such as the classifier implemented in *SExtractor*), especially at faint magnitudes: it increases the purity by up to 20% for stars and by up to 12% for galaxies, at i-magnitude fainter than 23.

Key words: Cosmology: observations – Surveys – methods : data analysis, neural networks, principal component analysis.

1 INTRODUCTION

What makes a star look different from a galaxy in a deep image? This seemingly very simple question hides the much more complicated issue of allocating a size and a scale to objects observed in the sky, which has concerned observers and theorists throughout the 20th century. The problem of classifying stars and galaxies in large scale surveys is a long-standing one. It has been encountered back in the early 1990's (e.g. the APM survey, Maddox et al. 1990) and poses a major challenge for all recent and large imaging cosmological surveys, including the Dark Energy Survey (DES) (http://www.darkenergysurvey.org/) and Euclid (http://sci.esa.int/euclid), which have been designed to uncover the nature of dark energy (DE). One common denominator of the wide variety of observational probes constraining DE is the necessity to select pure samples of galaxies. More specifically, all the surveys must differentiate galaxies at cosmological distances from local objects, to obtain pure, or at least well-understood, samples.

In the area of "precision cosmology", any source of systematic error is likely to play a decisive role and needs to be taken into account in order to refine the standard inflationary Big Bang picture. An example of a scientific question for which star/galaxy separation is a potentially critical systematic is the precision measurement of Primordial Non-Gaussianities (PNG). These manifest themselves by making the bias of a given type of tracers of dark matter halos strongly scale-dependent. This effect can easily be mimicked by any local systematic effect adding power at large scales and correlated with the galaxies. As the stellar distribution in the Milky Way is across large angular scales, star/galaxy separation is likely to introduce systematic errors in the measurement of PNG. Another example is the effect of occultation of galaxies by stars of comparable magnitudes. Ross et al. (2011) showed that this effect constitutes a source of systematic error in the measurement of angular and photometric distributions of luminous red galaxies. Photometric effects associated with faint stars could therefore partially account for the excess power seen in Thomas, Abdalla & Lahav (2011) for the MegaZ-LRG survey. This paper gives two other examples, in the case of Weak Lensing (WL) and Large Scale Structures (LSS) measurements, where star/galaxy separation is a key systematic, which needs to be taken into account in order to properly constrain DE.

The outline of this paper is as follows. In section 2, we present the Dark Energy Survey (DES) and the "DES-like" simulations which we base our analysis on. In section 3, we study the impact of star/galaxy misclassification on the measurement of the cosmological parameters, in the case of the WL and LSS probes, and show how the requirements on the statistical and systematic errors propagate into new requirements on the quality of star/galaxy separation. In section 4 we summarise the current methods for star/galaxy classification and the motivations for our multi-parameter approach. The details of the method are presented in section 5. In section 6, we compare our star/galaxy classification tool to the ones provided by other methods and confront these results to the science requirements derived in section 3. Finally, we summarise our main conclusions in section 7.

2 THE DARK ENERGY SURVEY

The Dark Energy Survey (DES)[1] is an imaging survey of 5000 sq-degrees on southern sky, utilising the four meter Blanco telescope in Chile. It will provide imaging of 300 million galaxies in five filters (g, r, i, z and Y). Photometric redshifts will be obtained from the colour information to produce a three dimensional survey. The main goal of DES is to determine the Dark Energy equation of state parameter, $w(z)$, and other key cosmological parameters to high precision. DES will measure $w(z)$ using four complementary techniques in a single survey: counts of Galaxy Clusters (GC) (with synergy with clusters detected by the Sunyaev-Zel'dovich effect with the South Pole Telescope), weak gravitational lensing (WL), galaxy power spectra and type Ia Supernovae (SNe). It is expected that the uncertainty on $w(z)$ will be only a few percent for each probe (see DES collaboration 2005, for detailed parameterisations and statistics). The science requirements of DES drove the construction of a new camera, DECam, which had its first light in September, 2012, and the survey will start in September, 2013.

As part of the process of testing and validation of the DES Data Management (DESDM) system (Mohr et al. 2012), a series of detailed simulations have been designed to serve as a test-bench for the development of the pipelines and for verifying the scientific reach of the experimental channels. Each of these iterations of the simulations are dubbed "Data Challenges" (DC). The simulation starts with the creation of galaxy catalogs stemming from an N-body simulation (Busha et al. 2013, in preparation) and detailed models of the Milky Way galaxy (Rossetto et al. 2011) for the star component. These are merged and fed to an image simulator which includes atmospheric and instrumental effects. The resulting images serve as inputs for DESDM and are processed as the data will be: the code *SExtractor* (Bertin & Arnouts 1996) produces a catalogue of more than 300 parameters encapsulating information about each detected object. This process is a joint effort of the Stanford, Brazil and Barcelona DES teams for the catalog side, and Fermilab for the image simulation aspect.

The most relevant features of these simulations for our study are:

- the seeing is introduced as a function of observing time;
- the shapes have been implemented using a Sersic profile which matches the observed profile;
- the Point Spread Function (PSF) takes into consideration the seeing for that time, the optics and the distortion as a function of separation from the optical axis.

The results shown in this paper are based on the latest release of simulated data, DC6, which covers approximately 140 square degrees to the full DES depth, corresponding to about 10 nights of observations. We select from it the objects with a model magnitude in the i band brighter than 24, as they are the ones most likely to be detected with DES. The average densities are approximately 10.4 galaxies and 4.8 stars per square arc-minute.

[1] http://www.darkenergysurvey.org/

3 SCIENCE REQUIREMENTS ON STAR/GALAXY SEPARATION

DES will be among the first surveys to combine in a single project the observation of the four preferred dark energy probes, as identified by the Dark Energy Task Force (DETF) (Albrecht et al. 2006). SNe and Baryonic Acoustic Oscillation (BAO) constrain the expansion of the Universe as a whole and are therefore referred to as *purely geometric*. WL and GC constrain both the expansion on the Universe and the growth of Large Scale Structures (LSS) (See Weinberg et al. 2013 for a complete review).

In order to properly constrain DE, the broad variety of measures carried out within each probe must meet certain requirements defined by DES science teams. While there is no unique way to specify the constraints on dark energy experiments and probes, the Figure of Merit (FoM), defined by the DETF, provides a useful metric. If we parameterise the time evolution of DE by the equation of state $w(a) = w_o + (1-a)w_a$, where $a(t) = \frac{1}{1+z(t)}$ is the cosmic scale factor and $z(t)$ is the redshift of an object emitting at time t, the FoM is defined as the reciprocal of the area of the error ellipse enclosing 95% confidence limit in the w_o-w_a plane. Larger FoM indicates smaller errors and therefore greater accuracy on the measurement of the parameters.

In other words, reaching the FoM goals requires to minimise the error on w_o and w_a. Since the total error is the sum of the *statistical* error and the *systematic* error, we can derive two types of science requirements. More concretely, the total Mean Square Error (MSE) on a cosmological parameter p_α can be decomposed as

$$MSE[p_\alpha] = \sigma^2[p_\alpha] + \Delta^2[p_\alpha] \, , \tag{1}$$

where $\sigma^2[p_\alpha]$ is the statistical error variance and $\Delta[p_\alpha]$ is the parameter shift due to the systematic signals. For each probe, both of these terms needs to be controlled in order to minimise the total error.

Star/galaxy misclassification is an interesting effect because it contributes to both the statistical and systematic part of the total error, for the WL and LSS probes. This allows us to translate separately the requirement on the statistical term (section 3.2) and the requirements on the systematic term (section 3.3) into requirements on the quality of the star/galaxy separation. Additional requirements are specific to each probe, e.g. PSF calibration for WL (section 3.4).

We outline below a formalism to derive these requirements.

3.1 Formalism

3.1.1 Completeness, contamination and purity

In the following, we define the parameters used to quantify the quality of a star/galaxy classifier. For a given class of objects, X (stars or galaxies), we distinguish the surface density of well classified objects, N_X, and the density of misclassified objects, M_X.

	True Galaxies	True stars
Objects classified as galaxies	N_G	M_S
Objects classified as stars	M_G	N_S

The galaxy *completeness* c^g is defined as the ratio of the number of true galaxies classified as galaxies to the total number of true galaxies. The stellar contamination f_s is defined as the ratio of stars classified as galaxies to the total amount of objects classified as galaxies.

$$c^g = \frac{N_G}{N_G + M_G} \, , \tag{2}$$

$$f_s = \frac{M_S}{N_G + M_S} \, . \tag{3}$$

The *purity* p^g is defined as $1 - f_s$:

$$p^g = \frac{N_G}{N_G + M_S} = 1 - f_s \, . \tag{4}$$

Similar parameters can be defined for a sample of stars: p^s, f_g and c^s.

We aim to formulate the requirements on the statistical and systematic errors in terms of constraints on these parameters. This will allow us to quickly compare the performance of the classifiers presented in section 4 and 5 and assess whether they allow us to achieve the goals of the DETF FoM.

One should note that there are some inefficiencies in the image pipeline, which are studied in DC6 and which we do not to deal with in this analysis. Instead, we define the latter parameters with respect to the truth tables. With real DES data, our results could be tested e.g. on HST data in the same fields.

3.1.2 Fisher Information Matrix

The Fisher information matrix describes how the errors on the angular power spectrum $C(l)$ (of the cosmic shear in the case of WL, and the density fluctuations of galaxies in the case of LSS) propagate into the precision on the cosmological parameters p_α . We employ this formalism (see Tegmark, Taylor & Heavens 1997, for a review), to quantify the impact of star/galaxy misclassification on each of the terms in equation 1, i.e. on the statistical and systematic errors on the cosmological parameters.

The Fisher matrix can be expressed as

$$F_{\alpha\beta} = \sum_l \sum_{(i,j)(m,n)} \frac{\partial C_{ij}(l)}{\partial p_\alpha} Cov^{-1}[C_{ij}(l), C_{mn}(l)] \frac{\partial C_{mn}(l)}{\partial p_\beta} \, , \tag{5}$$

where the sum is over multipole values and redshift bins (typically five for WL). $Cov[X, Y]$ designates the covariance matrix of X and Y and is given by (Takada & Jain 2004),

$$Cov[C_{ij}(l), C_{mn}(l)] = \frac{\{C_{im}(l)C_{jn}(l) + C_{in}(l)C_{jm}(l)\}}{f_{sky}(2l+1)\Delta l} \, , \tag{6}$$

where f_{sky} is the fraction of the sky covered by the survey ($f_{sky} = 0.1212$ for DES) and Δl is the width of the corresponding angular frequency bin.

3.2 Science requirements on the statistical errors

How does the need to control the statistical errors on the cosmological parameters propagate into a requirement on the quality of star/galaxy separation? In the following, we aim to answer this question in the case of the WL and LSS probes.

3.2.1 WL measurements

Gravitational lensing from distant intervening mass fluctuations causes the shapes of objects to be distorted such that they appear to be more or less elliptical. While no single object is intrinsically round, if the intrinsic shapes of galaxies are uncorrelated with one another, one can average the apparent shapes of many thousands of such objects to extract a distortion attributed to WL. The statistical properties of this observable pattern put a constraint on the power spectrum and therefore on the cosmological model and on DE. For some concise introductions to cosmic shear, see e.g. Refregier (2003), Mellier (1999) and Bartelmann & Schneider (2001).

How do star/galaxy misclassification affect the WL shear measurement? The predicted shear angular power spectrum $C_{ij}(l)$ depends on N_{eff}, the effective density per unit area of galaxies with reliable shape measurements,

$$C_{ij}(l) = \int_0^{r_H} dr r^2 W_i(r) W_j(r) P(l/r; r) + \delta_{ij} \frac{\sigma_e^2}{N_{eff}} \quad (7)$$

where $P(k = l/r)$ is the 3D matter power spectrum, $W_i(r)$ and $W_j(r)$ are the radial window functions of the redshift bins (i, j), r is the comoving distance and r_H is the Universe horizon. The angular power spectrum depends on N_{eff} through the last term, i.e. the "shot noise" due to σ_e, the intrinsic ellipticity noise for the galaxy sample.

In order study the effect of N_{eff} on the statistical error $\sigma[p_\alpha]$, we compute the Fisher matrix for different values of N_{eff}. We estimate the $C_{ij}(l)$ and $\frac{\partial C^g_{mn}(l)}{\partial p_\alpha}$ terms (see Eq. 5) using the same code as in Laszlo et al. (2011) and Kirk et al. (2011). The setup is as follows: we use a model with eight free parameters: $\{w_o, w_a, \Omega_m, H, \sigma_8, \Omega_b, n_s, b_g\}$; we assume a Planck prior (Jochen Weller, personal communication); there are five tomographic bins of roughly equal number density between z = 0 and 3; the redshift distribution is a Smail-type distribution (e.g. equation (12) of Amara & Refregier 2008, with $\alpha = 2$, $\beta = 1.5$, $z_0 = \frac{0.8}{1.412}$); we compute the $C_{ij}(l)$ and $\frac{\partial C^g_{mn}(l)}{\partial p_\alpha}$ terms for $l \in [1, 1024]$, to avoid the strongly non linear regime where baryon physics will start being important; and the photometric redshift error is $\Delta z = 0.05 * (1 + z)$.

We then compute the marginalized statistical error on the cosmological parameters by approximating them with their Cramer-Rao lower bound

$$\sigma[p_\alpha] \approx \sqrt{(F^{-1})_{\alpha\alpha}} \quad (8)$$

We show the results for w_o and w_a in figure 1 and for the other free parameters of our model in the Appendix.

Figure 1 shows that larger N_{eff} translates into smaller statistical errors on w_o and w_a, i.e. larger FoM, which puts a constraint on N_{eff}: it has to be higher than a threshold value N_{thresh} which can depend on the bandpass considered,

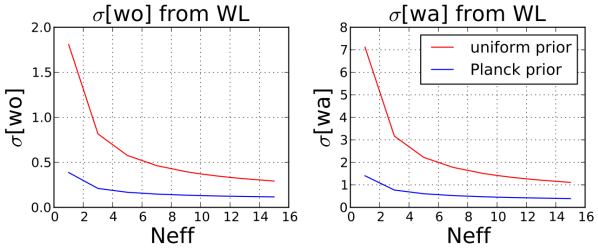

Figure 1. Marginalised statistical errors on the equation of state parameters w_o and w_a from the WL probe, for different values of the density of galaxies with reliable shape measurement N_{eff}. The errors are marginalised over $\{\Omega_m, H, \sigma_8, \Omega_b, n_s, b_g\}$ and computed using the assumptions and setup described in section 3.2.1. The red curve shows the errors computed with a non-informative prior whereas the blue curve is obtained assuming a Planck prior.

$$N_{eff} \geqslant N_{thresh} \, . \quad (9)$$

Figure 1 also shows that the curve levels off above $N_{thresh} = 10$, i.e. the effect of any variation of N_{eff} on the statistical error decreases at high N_{eff}. In practice, we request the increase of the statistical error due to star/galaxy missclassification to be smaller than 2%. This translates into a decrease of N_{eff} smaller than 4%, i.e.

$$c^g \geqslant 96.0\% \quad (10)$$

Star-galaxy misclassification is only one among many other sources of errors leading true galaxies to be rejected from the sample of galaxies with reliable shape measurements, (e.g., shape measurement errors and photo-Z errors). To insure that the statistical errors are controled, this condition on c^g should be completed by constraints on the survey parameters controling all the other sources of errors.

3.2.2 LSS measurements

LSS measurements allow us to constrain DE in various ways. The position of the BAO feature provides a standard ruler to study the expansion history. The shape of the angular power spectrum of the galaxy density fluctuation encapsulates precious information about the clustering amplitude and the growth of structures.

Star/galaxy misclassification affect the power spectrum measurements and the statistical error on the cosmological parameters in a similar way as in the WL case. Indeed, we can write the same equation as Eq. 7 for the angular power spectrum of the galaxy density fluctuations. The shot noise term is then given by $\frac{1}{N_G}$, where N_G is simply the surface density of detected galaxies. In figure 2, we show the evolution of the statistical errors on w_o and w_a with the density of detected galaxies, computed using the same setup as in the WL case.

In order to achieve the goals of the the LSS FoM, the 5000 sq-degrees DES survey will need to provide reliable photo-z and position measurement for about 200 millions galaxies, i.e. the number of galaxies correctly classified N_G should be higher than 11.1 per sq-arcminute (when using combined measurements from the r, i and z bandpasses).

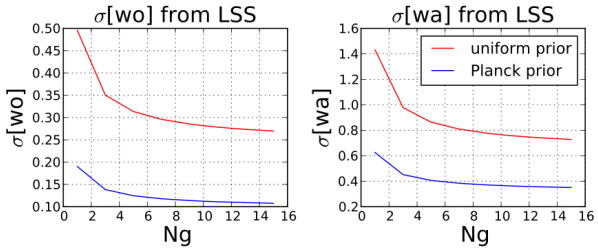

Figure 2. Marginalised statistical errors on the equation of state parameters w_o and w_a from the LSS probe, for different values of the density of detected galaxies N_g. The errors are marginalised over $\{\Omega_m,\ H,\ \sigma_8,\ \Omega_b,\ n_s,\ b_g\}$ and computed using the same assumptions and setup as in the WL case (see section 3.2.1), with $l \in [10, 400]$ (to avoid the non linear regime). The red curve shows the errors computed with a non-informative prior whereas the blue curve is obtained assuming a Planck prior.

When doing the latter calculation on the truth table of DC6, for which the surface density of galaxies is $N^g_{tot} \approx 12.5$, this threshold on N_G translates into the following requirement on the galaxy completeness provided by the star/galaxy classifier: $c^g > 88.9\%$.

Note that this requirement is a necessary but not sufficient condition, as other sources of errors, apart from star/galaxy misclassification (e.g. photo-z errors), reduce the number of galaxies which can be used for LSS measurement.

3.3 Science requirements on the systematic errors

We now explore the contribution of star/galaxy misclassification as a source of *systematic* error, which need to be controlled in order for the FoM objectives to be achieved. Star/galaxy misclassifications generate a residual signal $\delta C^{sys}(l)$ in the angular power spectra (of the cosmic shear in the case of WL, and the density fluctuations of galaxies in the case of LSS), which propagates into a systematic shift $\Delta[p_\alpha]$ of the cosmological parameter p_α. We use the same formalism as in Amara & Refregier (2008) (see also Kirk et al. 2012 and Huterer et al. 2006), to derive $\Delta[p_\alpha]$,

$$\Delta[p_\alpha] = \sum_{\beta,l,(i,j),(m,n)} (F^{-1})_{\alpha\beta}\delta C^{sys}_{ij}(l) Cov^{-1}[C^{gal}_{ij}(l), C^{gal}_{mn}(l)] \frac{\partial C^{gal}_{mn}(l)}{\partial p_\beta} , \quad (11)$$

where F^{-1} is the inverse Fisher matrix. A criterion usually used to constrain the contribution of the systematic error to the total MSE, is to define a tolerance on the systematics such that they do not dominate over statistical error. This is verified when

$$|\Delta[p_\alpha]| \leqslant \sigma[p_\alpha] , \quad (12)$$

In the following sections, we derive the systematic parameter shift for 7 cosmological parameters $p_\alpha = \{w_o, w_a, \Omega_m, H, \sigma_8, \Omega_b, n_s\}$ and the galaxy bias b_g, in the case of WL and LSS. This allows us to translate Eq. 12 into requirements on the quality of the star/galaxy separation.

3.3.1 Requirement from WL measurements

In the case of WL, the systematic error $\delta C^{sys}(l)$ comes from the fact that some stars are identified as galaxies, and therefore contribute to the measured cosmic shear. We decompose the measured shear γ_m into the contribution from the true galaxies and the contamination from the mixed stars,

$$\gamma_m = (1 - f_s)\gamma_g + f_s\gamma_s . \quad (13)$$

where $f_s = 1 - p^g$, is the stellar contamination rate (defined in Eq. 3).

The measured two-point shear correlation function is therefore

$$< \gamma_m\gamma_m >= (1 - f_s)^2 < \gamma_g\gamma_g > + f_s^2 < \gamma_s\gamma_s > , \quad (14)$$

where we assumed that γ_g and γ_s are uncorrelated.

In terms of measured angular power spectrum, the latter equation reads

$$C^{obs}(l) = (1 - f_s)^2 C^{gal}(l) + f_s^2 C^s(l) . \quad (15)$$

Therefore, the residual systematic signal is given by

$$\delta C^{sys}(l) = f_s^2(C^{gal}(l) + C^s(l)) - 2f_s C^{gal}(l) . \quad (16)$$

The requirement stated in Eq. 12 can be reformulated as a requirement on the stellar contamination rate f_s,

$$\mathcal{P}(f_s) \leqslant 0 , \quad (17)$$

where $\mathcal{P}$ is a second order polynomial.

The assumptions made to solve Eq. 17 are detailed below. We use the setup detailed in section 3.2.1 to compute the Fisher matrix and the marginalised statistical errors $\sigma[p_\alpha]$ on the cosmological parameters. To estimate $C^s(l)$ in Eq. 16, we assume it is the sum of a "shot noise" term and a term due to the correlation of stellar shapes across the field of view,

$$C^s(l) = C^s_{noise} + C^s_{tile}(l) \quad (18)$$

We measure $C^s_{tile}(l)$, the power spectrum of the shapes of the stars in DC6, using the same code as in Jarvis, Bernstein & Jain (2004). The "shot noise" term is given by

$$C^s_{noise} = \frac{\sigma_s^2}{N^s_{tot}} \quad (19)$$

where $N^s_{tot} = N_s + M_s$ (see section 3.1.1) is the density of stars and the ellipticity of stars, σ_s, is taken as the ellipticity of the PSF. To estimate σ_s, we use the *whisker length*. Given I_{xx}, I_{yy} and I_{xy}, the second moment of the light intensity from an object in x, y coordinates, a measure of the ellipticity of the light distribution is given by $e = (I_{xx} - I_{yy})(I_{xx} + I_{yy})$. The whisker length is then defined as $w \approx \sqrt{e(I_{xx} + I_{yy})} = \sqrt{e} \cdot r_{psf}$, where r^2_{psf} is given by $(FWHM)/2.35$. $FWHM$ designates the full width at half maximum and is given by $FWHM \approx 0.94$ in DES. In addition, the hardware has been designed with a requirement on the whisker length to be lower than a threshold value of 0.2" in the r, i and z band, which we take as an estimation of *whisk*. We get $C^s \approx 1.3187 \cdot 10^{-8}$ sr.

In Figure 3, we plot the two terms of the total error $MSE[p_\alpha]$ (see equation 1), i.e. the systematic parameter shift $\Delta[p_\alpha]$ due to star/galaxy misclassification, and the statistical error $\sigma[p_\alpha]$, for different values of the stellar contamination f_s and for each of the cosmological parameters of

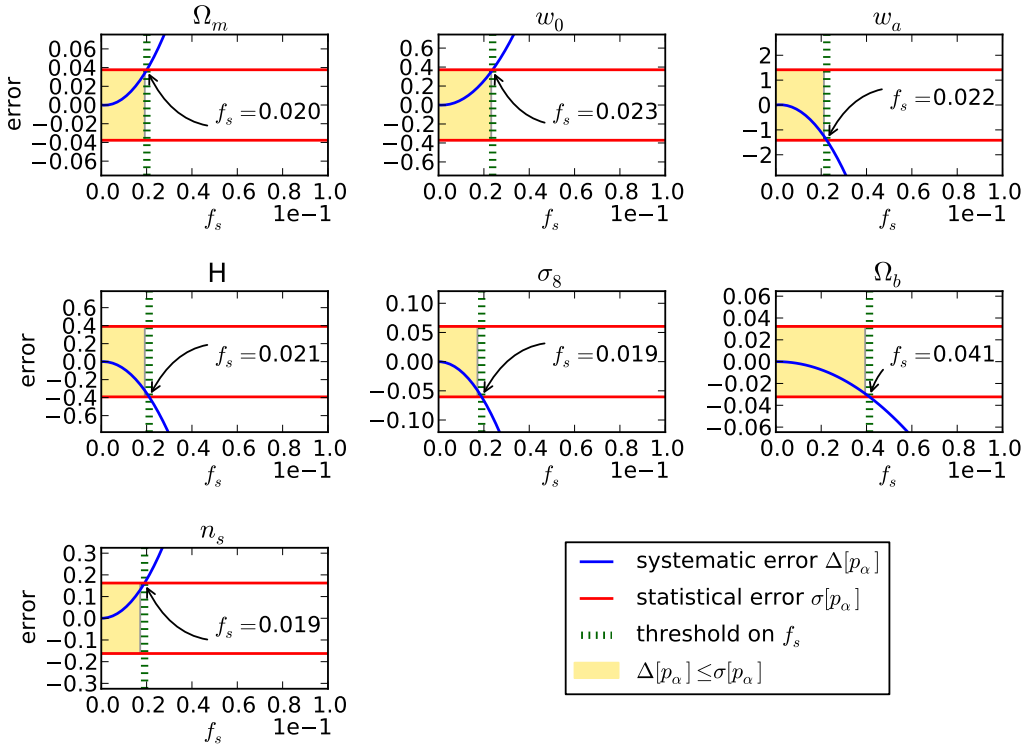

Figure 3. Marginalised statistical error σ (red line) and systematic parameter shift Δ (blue curve) from the WL probe, for different values of the stellar contamination f_s allowed by the star/galaxy classifier. Both σ and Δ are marginalised over $\{\Omega_m, H, \sigma_8, \Omega_b, n_s, b_g\}$ and are computed using the setup described in section 3.2.1. The yellow area corresponds to the values of f_s for which the requirement on the systematic errors is achieved, i.e. it does not dominate over the statistical error. This requirement translates into a threshold on f_s, indicated by the green line. Unlike LSS measurements, WL measurements are not sensitive to the galaxy bias b_g, which is the reason why it does not appear above.

our model $p_\alpha = \{w_o, w_a, \Omega_m, H, \sigma_8, \Omega_b, n_s, b_g\}$. In particular, for the equation of state parameters w_o and w_a, we find that we require $f_s \leqslant 0.022$. This translates into the following requirement on $p^g = 1 - f_s$, the purity provided by the star/galaxy classifier: $p^g \geqslant 97.8\%$.

Within an experiment designed to constrain DE such as DES, the constraints on the quality of star/galaxy separation comes from the need to control the errors on w_o and w_a. This being said, one should keep in mind that the contamination from stars affects the precision on the measurements of other cosmological parameters, as shown in figure 3.

3.3.2 Requirement from LSS measurement

Like for the WL probe, achieving the objectives of the LSS FoM requires the systematic error induced by star/galaxy misclassification to be smaller than the statistical error on w_o and w_a, and we can rewrite Eq. 12 in the case of LSS measurements. The shape of the residual systematic signal due to star/galaxy misclassification, δC^{sys}, is obtained following the same methodology as in the WL case, by decomposing the measured density fluctuation into the contribution from the true galaxies and the contamination from the stars identified as galaxies,

$$\delta_m = (1 - f_s)\delta_g + f_s\delta_s \ . \tag{20}$$

Replacing the shear angular power spectrum with the density fluctuation angular power spectrum in Eq. 16, we get the same requirement on the stellar contamination rate f_s as in Eq. 17. To estimate $C^s(l)$, we use the same stellar catalogue as used for the DES simulated sky survey produced by Busha et al. (2013, in preparation). We then calculate $C^s(l)$ using the approach from Thomas, Abdalla & Lahav (2010) and an adaptation of the HEALPix code (Gorski et al. 2005). We estimate the $C_{ij}(l)$ and $\frac{\partial C^g_{mn}(l)}{\partial p_\alpha}$ terms using the same code and setup as for the WL case. Figure 4 shows the systematic parameter shift induced by the stellar contamination, for each of the cosmological parameters of our model $p_\alpha = \{w_o, w_a, \Omega_m, H, \sigma_8, \Omega_b, n_s, b_g\}$. In particular, for the equation of state parameters w_o and w_a, we find that we require $f_s \leqslant 0.015$. This translates into the following requirement on $p^g = 1 - f_s$, the purity provided by the star/galaxy classifier: $p^g \geqslant 98.5\%$. The requirement on star/galaxy separation in a DE experiment is dictated by the need to accurately measure w_o and w_a. This being said, figure 4 demonstrates that these two parameters are not the most sensitive to the contamination by stars, which we leave for further analysis.

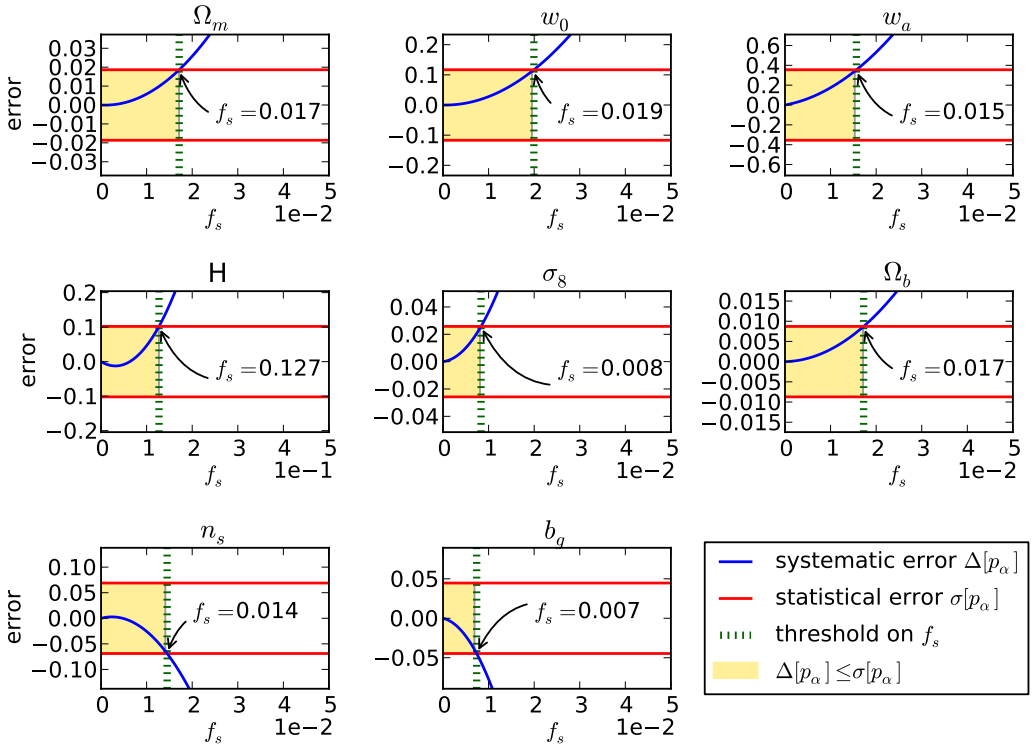

Figure 4. Marginalised statistical error σ (red line) and systematic parameter shift Δ (blue curve) from the LSS probe, for different values of the stellar contamination f_s allowed by the star/galaxy classifier. Both σ and Δ are marginalised over $\{\Omega_m, H, \sigma_8, \Omega_b, n_s, b_g\}$ and are computed using the setup described in section 3.2.1, with $l \in [10, 400]$, to avoid the non linear regime. The yellow area corresponds to the values of f_s for which the requirement on the systematic errors is achieved, i.e. it does not dominate over the statistical error. This requirement translates into a threshold on f_s, indicated by the green line. Unlike WL measurements, LSS measurements are sensitive to the galaxy bias b_g, as shown on the last panel.

3.4 Stellar PSF calibration for WL

In this section, we derive two additional requirements on the quality of the star/galaxy separation, from calibration constraints specific to the WL probe. The measured shapes of galaxies include a component due to the PSF of the combined telescope, atmosphere, and instrument which is correlated among galaxies. Removing this contribution requires careful measurement of the PSF, which is done using isolated stars. Therefore, additional requirements on star/galaxy separation come from PSF calibration for WL.

In order to determine the interpolation pattern of the PSF, one needs to find enough stars to adequately cover the area of the CCD chip. Based on preliminary studies of the DES science verification data, we believe around 200 stars per DES CCD is enough to adequately cover the area of the CCD chip and determine the interpolation pattern of the PSF. From the truth tables, we know that the total number of stars per CCD is approximately 810 and therefore the technical constraint on the completeness of the stars samples is $c^s \geqslant 25\%$.

In this analysis, we assumed that all non-saturated stars can be used for PSF estimation. In practice, the latter lower limit on the completeness could be more stringent because of detector non-linearities. Indeed, the "blooming" effect, caused by the voltages induced by the photons reaching the detector, leads brighter objects to appear larger than faint objects. This effect can lead to variations of the PSF between bright and faint stars, and therefore affect the PSF calibration. This reduces the number of stars available for PSF calibration.

The upper limit on the contamination in a sample of stars comes from the fact that galaxies will bias the inferred PSF, which in turn will bias the galaxy shapes. The target systematic error level for DES is 0.3%, which naively implies that this is the maximum fraction of galaxies in the stellar sample if each one causes an $O(1)$ error in the PSF estimates. However, galaxies that are erroneously tagged as stars do look like stars, so the induced systematic errors are more like $O(0.1)$. This means that we can tolerate a contamination of about 3%, which translates into a requirement on the purity: $p^s \geqslant 97\%$.

3.5 Summary of the science requirements star/galaxy separation

The requirements on the quality of the star/galaxy separation derived in this section are summarised in table 1.

A dedicated sample of stars is only needed when calibrating the PSF. Therefore, the two requirements on the samples of stars are only required for WL science. As far as samples of galaxies are concerned, LSS science requires

Table 1. Summary of the science requirements on the quality of star/galaxy separation.

	requirement from LSS	**from WL**
p^g	$\geqslant$ 98.5% (requirement on the systematic error)	$\geqslant$ 97.8% (requirement on the systematic error)
p^s	-	$\geqslant$ 97.0% (requirement on the PSF calibration)
c^g	$>$ 88.9% (requirement on the statistical error)	$>$ 96.0%(requirement on the statistical error)
c^s	-	$\geqslant$ 25% (requirement on the PSF calibration)

purer samples than WL science. This is due to star contamination affecting the corresponding measured "observable" in different ways. The contribution of misclassified stars to the measured shear is dominated by the shot noise term (see Eq. 18), which is approximately scale independent, whereas they mimic a l-dependent density fluctuation of galaxies and therefore contribute to the LSS measurement in a more complicated way. On the other hand, WL requires a more complete samples of galaxies. This is because a "usable" object means something different for LSS and WL. In order to be usable for LSS measurement, a galaxy needs to be detected with a reliable photometric redshift but WL also needs the shape of the galaxy to be measurable.

In the next sections, we will use these requirements to assess the performance of a new classifier, multi_class, and compare it to other classifiers currently used in galaxy surveys.

4 CURRENT TOOLS FOR STAR-GALAXY SEPARATION

Different strategies have been adopted to classify stars and galaxies in large sky surveys. The morphometric approach (e.g. Kron 1980; Yee 1991; Vasconcellos et al. 2011; Sebok 1979, Valdes 1982) relies on the separation of point sources (the ones most likely to be stars) from resolved sources (presumably galaxies). This approach is challenged at the faint magnitudes reached by the next generation of wide-field surveys, due to the vast number of unresolved galaxies.

Another strategy consists of using training algorithms. Machine learning distinguishes several types of learning strategies, Artificial Neural Network (ANN) being one successfully implemented example of *supervised learning*. ANN has previously been applied to the star/galaxy separation problem (e.g. Odewahn et al. 1992, Naim 1995, Bertin & Arnouts 1996). Indeed, star/galaxy separation shares with many other classification problems the three criteria which usually make neural computing applications particularly successful:

- The task is well-defined in that we know precisely what we want, i.e. classify objects in two distinct classes.
- There is a sufficient amount of data available to train the net to acquire a useful function based on what it should have done in these past examples.
- The problem is not of the type for which a rule base could be constructed, and which therefore could more easily be solved using a symbolic Artificial Intelligence approach.

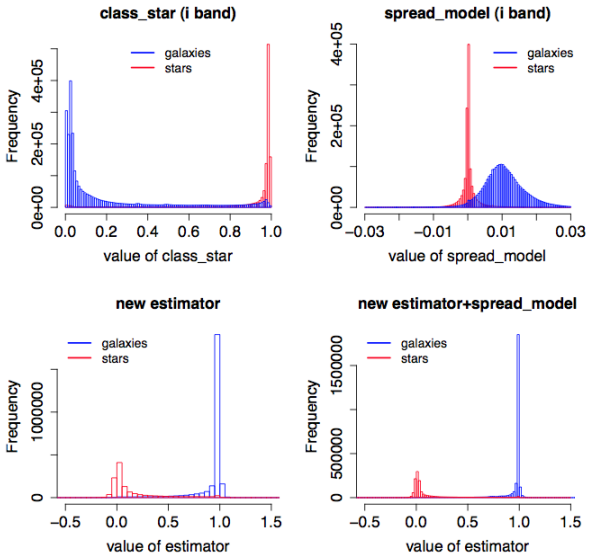

Figure 5. Distribution of the output of all the classifiers presented in the paper. The two upper histograms show the classification performed by class_star and spread_model. The lower histograms show the classification performed by our new estimator, multi_class. On the right one, we incorporate X_{spread_model} in the input parameters of the ANN. The advantages of plugging X_{spread_model} into our tool are explained in section 5.3.2. This allows an increase of the purity for a given completeness, as shown in figure 9.

Other supervised classifiers, such as Support Vectors Machine (SVM), have been more recently used for the star/galaxy separation problem, as well as unsupervised tools such as Hierarchical Bayesian techniques (e.g. Fadely, Hogg & Willman 2012).

Throughout this section, we will use the following notations to define:

- *classification tools* - class_star; spread_model and multi_class
- *classification output* - X_{class_star}; X_{spread_model} and X_{multi_class} .

As described below (section 4.1), class_star and spread_model are two classifiers currently implemented in *SExtractor* (Bertin & Arnouts 1996) and in the next sections we present a new method for star/galaxy separation called "multi_class", designed to achieve the science requirements derived in section 3 at the faint magnitudes reached by DES.

4.1 Current approaches

Both the morphometric and the training approaches are implemented in *SExtractor* (Bertin & Arnouts 1996), with two classifiers, class_star and spread_model.

4.1.1 The training approach - class_star

The first classifier to be implemented in *SExtractor* was class_star. Its performance on our example sub-survey is

shown in figure 5. It uses a set of features of the objects as the input space for a built-in previously trained ANN. These parameters are:

(i) eight isophotal areas, at regular intervals spanning from the detection threshold to the intensity peak;
(ii) the intensity peak;
(iii) the local value of the seeing.

This specific pre-defined set of inputs, chosen mainly for historical reasons, is the main weakness of the class_star estimator. The choice of training the ANN on isophotal areas (normalised to the local PSF footprint area) makes it sensitive to close pairs of objects (star-star, star-galaxy, galaxy-galaxy) either blended or de-blended. Since star-star pairs are common on the bright end of the source population, the classifier has a tendency to miss bright, compact galaxies.

More generally speaking, given the large amount and diversity of information encapsulated in the parameters provided by *SExtractor*, this specific choice of inputs has become hard to justify as it is using a very small part of the available information. The photometry, the shape or the size of an object should also be useful indicators of whether it is a star or a galaxy.

Class_star has the advantage of making use of several parameters and combining the information they contain. In this sense it is a "multi-parameter" estimator. However, it does not use the most relevant parameters. A more flexible and sensible choice of the inputs is likely to give much better results. This is the main motivation for the new approach tested in this paper.

4.1.2 The morphometric approach - spread_model

The classifier implemented in recent development versions of *SExtractor*, spread_model (Desai et al. 2012, Bertin et al. in preparation), takes a morphometric approach. It carries out diverse operations directly on the image pixels with no use of the object's parameters generated by *SExtractor*. The newest version of spread_model acts as a linear discriminant between the best fitting local PSF model ϕ and a slightly "fuzzier" version made from the same PSF model, convolved with a circular exponential model with scale length given by $FWHM/16$ (FWHM being the Full-Width at Half-Maximum of the local PSF model). Spread_model is normalized to allow for comparison of sources with different PSFs throughout the field. It is defined as

$$\mathrm{X}_{\mathrm{spread\_model}} = \frac{\phi^T W x}{\phi^T W \phi} - \frac{G^T W x}{G^T W G} \,, \qquad (21)$$

where x is the image centred on the source, W is the inverse of its covariance matrix which is assumed to be diagonal, ϕ is the PSF and G is the circular exponential model convolved with the PSF. By construction, spread_model is close to zero for point sources (most likely to be stars), positive for extended sources (most likely to be galaxies) and negative for detections smaller than the PSF, such as cosmic ray hits.

The performance of this late version of spread_model on our example sub-survey is shown in figure 5. Although this morphometric approach is quite efficient, it is not entirely satisfying as it does not make use of any of the 300 *SExtractor* parameters, which are likely to encapsulate lots of relevant information for star/galaxy separation.

5 THE MULTI_CLASS METHOD

5.1 Motivation and principle

Our goal is to combine the assets of both the morphometric approach and the training approach. We adopt the multi-parameter approach allowed by the training method and focus on making the optimal choice of input parameters. The steps of the method are as follows:

(1) Optimal choice of input parameters using a PCA;
(2) Training and running an ANN.

5.2 Step 1- optimal choice of input parameters using Principal Component Analysis

We make a broad pre-selection of all the parameters likely to be relevant for star/galaxy classification. These parameters are listed in table 2. They include:

(i) **photometry** in 5 bands (g,r,i,z and y);
(ii) the **size** of objects;
(iii) the **shape** of objects;
(iv) the **surface brightness** of objects;
(v) qualifiers of the **fitting** procedure;
(vi) the **output of the class_star classifier**, X_{class_star};
(vii) additional **analysis-dependent information**.

Ideally, we could run an ANN with this full set of relevant inputs. In practice, training the ANN is a non-linear iterative process, which becomes more time consuming and less robust as the number of input parameters increases. In fact, defining an optimal set of input parameters consists of minimising its size while maximising the amount of relevant information it contains.

Our initial set of parameter is redundant, as many of the parameters within each sub-group are dependent variables. For example, we show in figure 6 the dependencies between four types of magnitudes parameters measured in a given band. In order to reveal the redundancies within the data and compress it, we use a Principal Component Analysis (PCA). This statistical method, which comes down to diagonalising the covariance matrix of the data, allows us to re-express the pre-selected parameters detailed above in a more meaningful basis of orthogonal, i.e. uncorrelated variables called *principal components*. The first principal component is chosen to account for most of the data variability and thus to have the highest possible variance. Then each succeeding principal component has the highest possible variance under the constraint of being orthogonal - that is uncorrelated - to the preceding one.

We run several "well-informed" PCAs on sub-ensembles of parameters, rather than a "blind" PCA on the full set of initial parameters. We choose to group in these sub-ensembles parameters which have the same units (or measure) and which are linearly dependent on each other (such as the magnitudes in a given band, as shown in figure 6). Indeed, when the parameters are linearly dependent, PCA is successful at finding a new basis of meaningful independent variables.

Table 2. DC6 pre-selected parameters, grouped as defined in section 5.2, by type of information they provide: (i): photometry; (ii) size; (iii): shape; (iv): surface brightness; (v): qualifiers of the fitting procedure; (vi): output of the class_star classifier; (vii): additional analysis-dependent information. It should be noted that all of these parameters are distance-dependent. The need for K-correction to the magnitudes is therefore dealt with by including the photometric redshift in this pre-selected parameters space.

	Parameters	**Description**
(i)	mag_aper_ in 5 bands	Fixed aperture magni--tude with 6 different apertures
	mag_auto in 5 bands	Kron-like elliptical aperture magnitude
	mag_iso in 5 bands	Isophotal magnitude
	mag_model in 5 bands	Magnitude from model-fitting
	mag_petro in 5 bands	Petrosian-like elliptical aperture magnitude
	mag_psf in 5 bands	Magnitude from PSF-fitting
	mag_spheroid in 5 bands	Spheroid total magn--itude from fitting
(ii)	kron_radius (from the detection image)	Kron apertures
(iii)	ellipticity (from the detection image)	$1 - B_{image}/A_{image}$
(iv)	isoarea_world in 5 bands	Isophotal area above analysis threshold
	FWHM_world in 5 bands	FWHM assuming a gaussian core
(v)	chi2_model in 5 bands	Reduced chi-square of the fit
	chi2_psf in 5 bands	Reduced chi-square from PSF-fitting
	niter_model in 5 bands	Number of iterations for model-fitting
(vi)	X_{class_star} in 5 bands	Output from class_star
(vii)	nlowdweight_iso	Number of pixels with low detection weight over the isophotal profile
	photoZ	photometric redshift

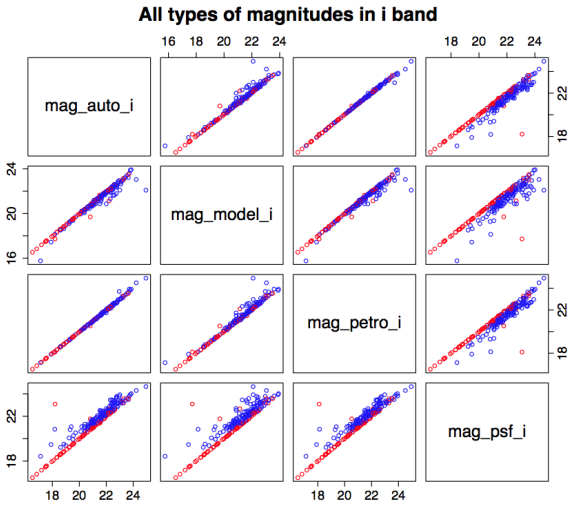

Figure 6. Scatter plots for stars (red markers) and galaxies (blue markers), for four different types of magnitudes in the i band. The magnitudes are strongly correlated and PCA is therefore well adapted to re-express them in a new basis of independent variables.

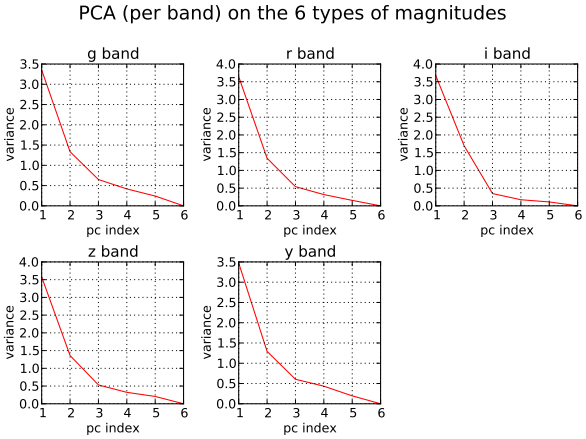

Figure 7. Value of the variance of the principal components as a function of their index for the fives (per-band) PCAs performed on the six types of magnitudes: *mag_auto*, *mag_iso*, *mag_model*, *mag_petro*, *mag_spheroid* and *mag_psf*.

Our new set of parameters includes uni-band parameters from the initial set (such as the photometric redshift or the ellipticity), as well as the principal components from the PCAs listed below:

- PCA on the five bands of each multi-band parameter;
- PCA on the six fixed-aperture magnitudes in each band;
- PCA on the six other types of magnitudes in each band (i.e. *mag_auto*, *mag_iso*, *mag_model*, *mag_petro*, *mag_spheroid* and *mag_psf*).

Figure 7 shows the variances of the principal components of these six types of magnitudes in each band as a function of their index. Each of these PCAs shows that most of the variance of the data is encapsulated in a reduced number of principal components. In many cases, using PCA for data reduction consists of selecting only the principal components with the highest variance and approximating the data by its projection on this smaller set of variables. This encompasses the assumption that the important information is represented by the components with the highest variances. In the case of star/galaxy separation, this assumption is too simplistic. Indeed, the class of an object is only one possible source of variance and high variance could also be due to differences between objects in a given class. Therefore, when looking for the most relevant components for star/galaxy separation, we need another criterion to quantify their aptitude to separate between the classes. We calculate the *Fisher discriminant* (Fisher 1936) for each of the new parameters, defined as the inter-class variance over the intra-class vari-

ance,

$$\mathcal{F}_i = \frac{(\overline{X_{G,i}} - \overline{X_{S,i}})^2}{\sigma^2_{G,i} + \sigma^2_{S,i}} \ , \quad (22)$$

where $\overline{X_{A,i}}$ is the empirical mean value of the i^{th} parameter for class A and $\sigma^2_{A,i}$ is its empirical variance. Figure 8 shows the classification performed by the three parameters with the highest Fisher discriminant. The fifteen parameters with the highest Fisher discriminant form our final set of input parameters for the ANN (as dicussed in section 5.3.1, more than twenty input parameters make the ANN less robust, so we limit the basic set to fiftenn parameters, in anticipation of the other five that will be added in section 5.3.2).

5.3 Step 2 - running an ANN on the optimal inputs space

Once a set of optimal parameters is defined, the next step consists of mapping these parameters to the class of the objects. This mapping is performed by training an ANN.

5.3.1 ANN: principle and advantages

In essence, an ANN is a highly-flexible, fully non-linear fitting algorithm. During the training phase, it receives a set of input patterns and a given property (in our case the class of the object), which needs to be fitted to them. The training consists of several iterations during which a number of free parameters known as *weights* are adjusted so as to minimise the difference between the outputs of the neural network for each pattern and the desired property. The algorithm then learns how to link the inputs to the desired property. After the training phase, the ANN can be used to infer this property from a set of input objects for which it is unknown. For our analysis, we train an ANN to map the set of optimal input parameters selected in section 5.2 to the class of the object (star or galaxy) on a sample of objects for which the answer is known (the training is made on the DC6 simulations for which we know the true class of each object). The ANN is then used to deduce the class of a distinct set of objects.

An ANN is made of computing units called *neurons*, arranged in several layers and connected by synapses in which the information flows in a single direction. The complexity of the network depends on the number of layers and neurons in each layer. We chose to use the ANNz photometric redshift code (Collister & Lahav 2004) , which was originally designed for photometric redshift measurements, but can be effectively and straightforwardly applied to our classification problem. The trade-off between the complexity of the network and its performance has been investigated by Firth et al. (2003). For the same number of parameters, adding extra hidden layers is found to give greater gains than widening existing layers. As the network complexity is increased, the accuracy eventually converges so that no further improvement is gained by adding additional nodes. We chose a network architecture with an input layer of fifteen parameters (or twenty, as explained in the next section) and two hidden layers of twenty nodes, which turns out to be sufficiently complex for such convergence to be achieved.

Training on real data, as opposed to simulations, is preferable, yet more challenging. One option would be to use data from space-based surveys, as in space the PSF is not affected by the seeing. Data from the Hubble Space Telescope could be used to train our tool for the real DES survey data.

5.3.2 Plugging other classifiers in the method

Using an ANN brings flexibility to the training approach. It allows us not only to choose which inputs to use, but also in what number. In particular, we can take the output of other classifiers as inputs to our method.

We run a PCA on the five X_{class_stars} (in the five bands). Not surprisingly, the first principal component has a high Fisher discriminant (as shown in figure 8) and is therefore included in the 15 input parameters selected in section 5.2. As the the five bands of X_{spread_model} are less clearly linearly dependent, we choose not to run a PCA on them and add the five X_{spread_model} to the set of fifteen input parameters, which amounts to twenty input parameters.

Figure 9 presents the purity level at a given completeness for these two different configurations of our method. The performance of our method with fifteen input parameters (orange curve) can be compared to the performance when plugging in X_{spread_model} (pink curve). Including X_{spread_model} in the inputs allows an increase in the level of the purity by 2% at faint magnitudes. Running the ANN on the fifteen preselected parameters (orange curve) already gives better results than spread_model (blue curve) for most of the magnitude range (except for the very faint magnitudes, in the galaxies case). However, the best results are obtained by combining the two, i.e by running the ANN on a hybrid input space combining the 15 selected parameters and X_{spread_model}.

6 CLASSIFICATION RESULTS

We showed that we can optimise our classifier performance by using a "well-informed" PCA strategy (section 5.2), and by incorporating X_{spread_model} into the method (section 5.3.2). We now compare our classifier performance to the one of the other classifiers. We will focus on comparing multi_class to spread_model, as the performance of class_star is widely surpassed by both spread_model and multi_class for most of the magnitude range (as shown in Figure 9).

For LSS, our new classifier allows us to achieve requirements which cannot be fulfilled by spread_model. Figure 10 shows that the 98.5% limit on p^g (derived in section 3.3.2 and shown in purple on the figure) cannot be reached by spread_model, whereas multi_class allows us to reach it up to magnitudes of 22.9 (at the required 88.9% completeness level, derived in section 3.2.2).

For WL, multi_class allows us to increase the magnitude limit below which the science requirements are achieved. Figure 9 shows that this magnitude limit increases from 21.5 to 23.4 for the requirement on the stars purity p^s, and from 22.0 to 22.9 for the requirement on the galaxy purity p^g. Figure 10 and figure 11 generalise this to a broad range of

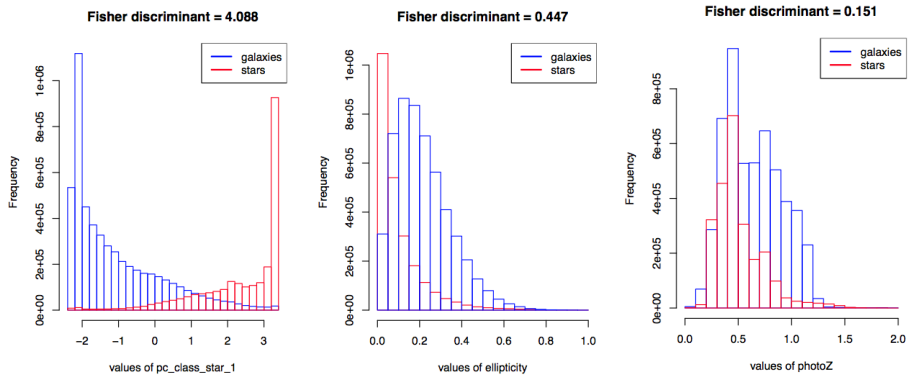

Figure 8. Distribution of the three parameters with the highest Fisher discriminant, for stars and galaxies as indicated in the figure. *pc_class_star_1* (left) is the first principal component from a PCA performed on the five bands of X_{class_star} (see section 5.3.2). The two other parameters shown, *ellipticity* (centre) and *photoZ* (left) have not gone through any PCA.

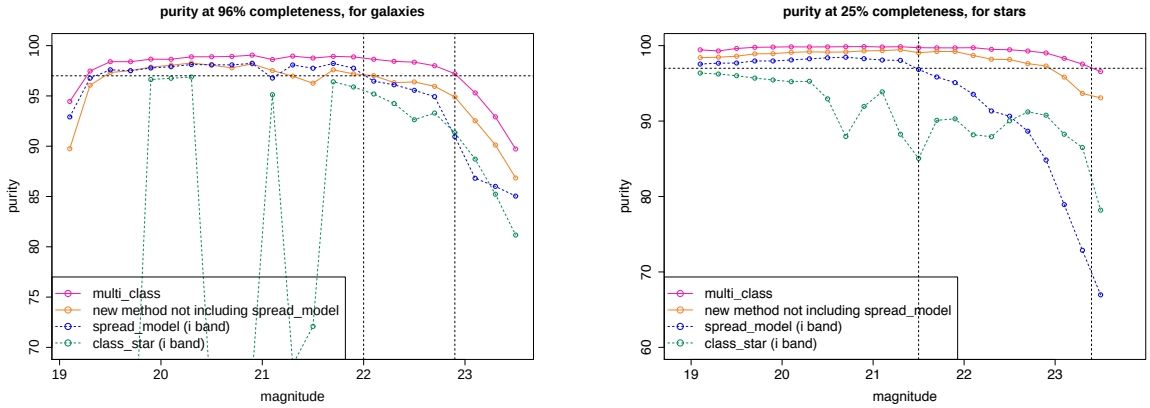

Figure 9. Purity level at the required completeness, for the WL probe, as a function of magnitude in the i band. The orange and pink curves correspond to different versions of our method, whereas the blue and green ones show the performance of the classifiers class_star and spread_model. The orange curve is obtained when running the ANN on the 15 parameters selected in section 5.2 and the pink curve, the final version of multi_class, is obtained when adding spread_model in five bands to this set of inputs. The dashed horizontal line shows the science requirement from WL science on p^g (97.8%, section 3.3.1) and p^s (97.0%, section 3.4). The requirement on p^g is achieved by multi_class up to magnitudes of 22.9, whereas spread_model only allows us to reach 22.0. The requirement on p^s is achieved up to magnitudes of 23.4 with multi_class, versus 21.5 with spread_model.

completenesses. In figure 12, we consider the improvement in the purity of a sample of stars and a sample of galaxies, as a function of magnitude, for a large range of completenesses. At faint magnitudes - typically fainter than 23 - multi_class improves the purity achieved by spread_model by up to 12% for galaxies and by up to 20% for stars.

7 CONCLUSIONS

We showed that star/galaxy misclassification contributes to both the statistical and systematic error on the measurement of cosmological parameters. In particular, it affects the measurement of the DE equation of state parameters, w_o and w_a, which future large photometric surveys such as DES aim to measure accurately. In the case of WL and LSS measurements, we translated the DETF FoM requirements on the statistical and systematic errors and the constraints from PSF calibration into the corresponding science requirements on the quality of star/galaxy separation. We formulated these requirements using two parameters: the purity and completeness of classified samples of stars and galaxy.

In order to meet these new requirements, we built an efficient method for star/galaxy classification, called multi_class, which combines a PCA with a learning algorithm. Our multi-parameter approach allows us to make use of the huge amount of information provided by *SExtractor*. In particular, the use of PCA allows us to better understand the correlations in the data, and to implement this physical knowledge in the classifier.

In ground-based surveys such as DES, the image quality is not constant with position and therefore any purely morphometric method gives limited performance, especially at faint magnitudes. The flexibility of using an ANN allows us to consider the morphometry as one input parameters among many others and to integrate the performance of other classifiers to our new tool. Our new classifier, multi_class, significantly improves the performance

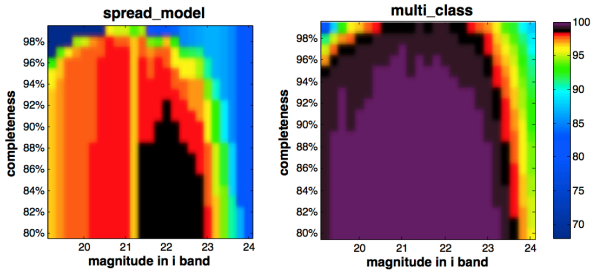

Figure 10. Level of purity for a sample of galaxies p^g, for different magnitudes and values of the completeness. The 98.5% level requirement from LSS (section 3.3.2) is shown in purple, and the 97.8% limit required for WL (section 3.3.1) is shown in black. Spread_model does not allow to achieve the LSS requirement, which multi_class can reach. Multi_class also allows us to achieve the requirement from WL at fainter magnitudes than spread_model.

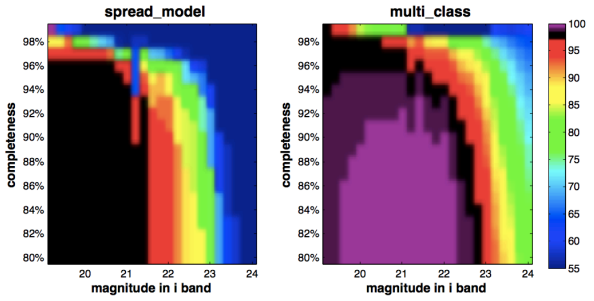

Figure 11. Level of purity for a sample of stars p^s, for different magnitudes and values of the completeness. The 97% science requirement (from WL, derived in section 3.4) is shown in black. Higher purity levels are shown in purple and light purple. Our new estimator, multi_class, allows us to widen the range of both magnitude and completeness where this requirement is achieved.

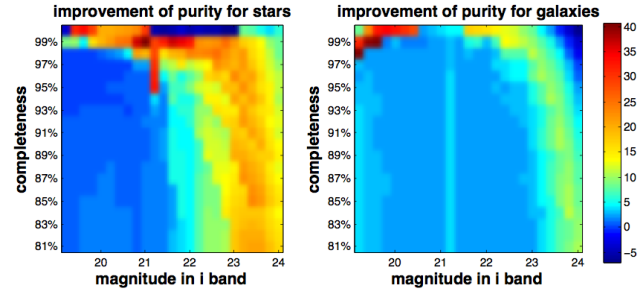

Figure 12. Difference of the purity level achieved by multi_class and spread_model, $p_{multi\_class} - p_{spread\_model}$ for stars (left) and galaxies. At faint magnitudes (ranging from 23 to 24), multi_class allows us to increase the level of p^s achieved by spread_model by up to 20%, and p^g by up to 12%.

of the morphometric classifier implemented in *SExtractor* (spread_model), which cannot achieve the LSS science requirements on star/galaxy separation. For both the LSS and WL probes, it allows us to widen the range of both magnitude and completeness where the derived science requirements are achieved. For magnitudes fainter than 23, multi_class improves the purity achieved by spread_model by up to 12% for galaxies and by up to 20% for stars.

DES will begin survey operations in September, 2013, and will be running for five years. Therefore, we should be able to test the results shown in this paper on real data in the near future. The faint magnitudes reached by this new classifier constitute an important asset, which should allow to achieve the science requirements on star/galaxy separation in the next generation of wide-field photometric surveys.

ACKNOWLEDGMENTS

MTS would like to thank Gary Bernstein for his usefull comments and advice, Adam Hawken for his great explanations, Alexandre Refregier for a very useful discussion, and Ashley Ross, Manda Banerji, Alex Merson, Foteini Oikonomou, Boris Leistedt, Sreekumar Balan and Iftach Sadeh for their input to the project. MTS is grateful for the support from the University College London Perren and Impact studenships. FBA acknowledges the support of the Royal Society via a University Research Fellowship. OL acknowledges a Royal Society Wolfson Research Merit Award, a Leverhulme Senior Research Fellowship and an Advanced Grant from the European Research Council. BR acknowledges support from the European Research Council in the form of a Starting Grant with number 240672. We acknowledge UK's STFC for supporting DES optics and science.

Funding for the DES Projects has been provided by the U.S. Department of Energy, the U.S. National Science Foundation, the Ministry of Science and Education of Spain, the Science and Technology Facilities Council of the United Kingdom, the Higher Education Funding Council for England, the National Center for Supercomputing Applications at the University of Illinois at Urbana-Champaign, the Kavli Institute of Cosmological Physics at the University of Chicago, Financiadora de Estudos e Projetos, Fundao Carlos Chagas Filho de Amparo Pesquisa do Estado do Rio de Janeiro, Conselho Nacional de Desenvolvimento Cientfico e Tecnolgico and the Ministrio da Cincia e Tecnologia, the Deutsche Forschungsgemeinschaft and the Collaborating Institutions in the Dark Energy Survey.

The Collaborating Institutions are Argonne National Laboratories, the University of California at Santa Cruz, the University of Cambridge, Centro de Investigaciones Energeticas, Medioambientales y Tecnologicas-Madrid, the University of Chicago, University College London, DES-Brazil, Fermilab, the University of Edinburgh, the University of Illinois at Urbana-Champaign, the Institut de Ciencies de l'Espai (IEEC/CSIC), the Institut de Fisica d'Altes Energies, the Lawrence Berkeley National Laboratory, the Ludwig-Maximilians Universitt and the associated Excellence Cluster Universe, the University of Michigan, the National Optical Astronomy Observatory, the University of Nottingham, the Ohio State University, the University of Pennsylvania, the University of Portsmouth, SLAC, Stanford University, the University of Sussex, Texas A&M University, and the Institute of Astronomy at ETH-Zurich.

REFERENCES

Albrecht A. et al. 2006, arXiv:astro-ph/0609591
Amara A., Refregier A., 2008, MNRAS, 391, 228
Bartelmann M., Schneider P., 2001, Phys.Rept, 340, 291

Bertin E., Arnouts S., 1996, A&A, 393, 404
Bertin E., in preparation.
Busha M., 2013, in preparation.
Collister A., Lahav O., 2004, PASP, 345, 351
Collister A., Lahav O., 2007, MNRAS, 68, 76
DES Collaboration, 2005 astro-ph/0510346
Desai S. et al., 2012, arXiv:1204.1210
Fadely R., Hogg D. W., Willman B., 2012, arXiv:1206.4306v2
Firth A. E. et al., 2003, MNRAS, 1195,1202
Fisher R. A., 1936, Annals of Eugenics, 179, 1936
Gorski K. M. et al., 2005, AJ, 622, 759
Henrion M., Mortlock D. J., Hand D. J., Gandy A., 2011, MNRAS, 412, 2286
Hinshaw G. et al., 2012, arXiv:1212.5226
Huterer D. et al., 2006, MNRAS, 366, 101
Jarvis M., Bernstein G., Jain N., 2004, MNRAS, 352, 338
Jarvis M., Jain B., 2004, 2004astro.ph.12234J
Joachimi B., Bridle S., L., 2010, A&A, 523: A1
Kirk D., et al., 2011, arXiv:1109.4536v2
Kirk D., et al., 2012, MNRAS, 424, 1647
Kron R. G., 1980, ApJS, 43, 305
Laszlo I. et al., 2011, arXiv:1109.4535v1
Maddox S. J. et al., 1990, MNRAS, 643, 318
Mellier Y., 1999, ARA&A, 37, 127
Mohr J. J. et al., 2012, arXiv:1207.3189v1
Naim, A. , PhD thesis "The Application of Artificial Neural Network to Astronomical Classification", University of Cambrige, 1995.
Odewahn S. C. et al., 1992, AJ, 103, 692
Refregier A., 2003, ARA&A, 41, 645
Refregier A., Amara A., Kitching T.D., Rassat A., 2011, A&A, 528
Ross A. et al., 2011, MNRAS, 1350, 1373
Rossetto B. M. et al., 2012, AJ, 141, 185
Sebok W. L., 1979, AJ, vol. 84,1526, 1536
Takad M., Jain B., 2004, MNRAS, 348, 897
Tegmark M., Taylor A. N., Heavens A. F., 1997, ApJ, 480, 22
Thomas S., Abdalla F. B., Lahav O., 2010, MNRAS, 1669,1685
Thomas S., Abdalla F. B., Lahav O., 2011, Phys. Rev. Lett., 106.241301
Valdes F., 1982, SPIE, 465, 472
Vasconcellos E. C. et al., 2011, AJ, 141, 189
Weinberg et al., 2013, arXiv:1201.2434v2
Yee H. K. C., 1991, PASP, 103, 396

APPENDIX A: STATISTICAL ERRORS ON THE COSMOLOGICAL PARAMETERS {Ω_M, H, σ_8, Ω_B, N_S, B_G} FROM WL AND LSS MEASUREMENTS

In the following, we show the marginalised statistical errors on $\{\Omega_m, H, \sigma_8, \Omega_b, n_s, b_g\}$ from the WL probe (Figure A1) and the LSS probe (Figure A2), for different values of the density of galaxies with reliable shape measurement N_{eff} and of the density of detected galaxies N_G respectively. The errors are marginalised and computed using the assumptions and setup described in section 3.2.1, with $l \in [1, 1024]$ in the WL case and with $l \in [10, 400]$ in the LSS case. The red curve shows the errors computed with a non-informative prior whereas the blue curve is obtained assuming a Planck prior.

This paper has been typeset from a TEX/ LATEX file prepared by the author.

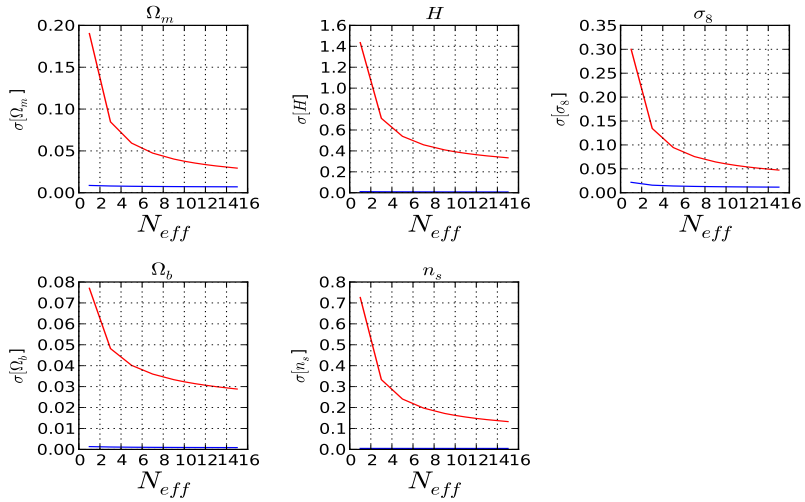

Figure A1. Marginalised statistical errors on $\{\Omega_m,\ H,\ \sigma_8,\ \Omega_b,\ n_s,\ b_g\}$ from the WL probe.

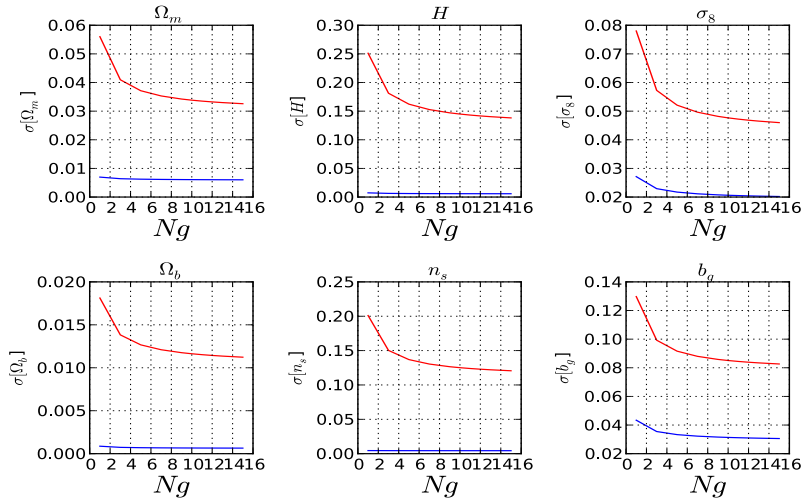

Figure A2. Marginalised statistical errors on $\{\Omega_m,\ H,\ \sigma_8,\ \Omega_b,\ n_s,\ b_g\}$ from the LSS probe.